Multiple Ordered Phases in a Block Copolymer Melt

K. Almdal,† K. A. Koppi, and F. S. Bates*

Department of Chemical Engineering and Materials Science, University of Minnesota, Minneapolis, Minnesota 55455

K. Mortensen

Risø National Laboratory, Roskilde, Denmark

Received July 22, 1991; Revised Manuscript Received November 5, 1991

ABSTRACT: A poly(ethylenepropylene)–poly(ethylethylene) (PEP–PEE) diblock copolymer containing 65% by volume PEP was investigated using small-angle neutron scattering (SANS) and rheological measurements. Four distinct phases have been identified as a function of temperature: three ordered phases at low temperatures and a disordered phase at elevated temperatures. Evaluation of the ordered phases was facilitated by the introduction of long-range order using a shear-orientation technique. SANS data were acquired as a function of temperature for three specimen orientations corresponding to the principle Cartesian axis associated with the shear-orientation direction. Dynamic rheological properties were determined using a simple shear geometry with the strain direction coincident with the direction of macroscopic orientation. The order–disorder and order–order transitions were determined to be first-order based on discontinuities in the SANS pattern symmetries and intensities and dynamic elastic moduli. At the lowest experimental temperatures the material exhibits a (rippled) lamellar phase. At intermediate temperatures two new ordered phases appear. Above the order–disorder transition temperature a fluctuating disordered state exists. The microstructure of the two intermediate phases has not been conclusively determined although the rheological and SANS results rule out the classical morphologies. These findings are inconsistent with the generally accepted concept of universal block copolymer phase behavior based on composition and χN alone, where χ and N are the Flory–Huggins interaction parameter and degree of polymerization, respectively.

Introduction

Numerous experimental and theoretical studies over the past 2 decades have led to a well-developed understanding of block copolymer thermodynamics as described in a recent review article.[1] Equilibrium phase behavior is usually expressed in terms of the polymer composition f and the reduced parameter χN where χ represents the Flory–Huggins segment–segment interaction parameter and N refers to the overall degree of polymerization. Nearly all the quantitative experimental evidence regarding the block copolymer phase diagram has been obtained from transmission electron microscope and small-angle X-ray and neutron scattering measurements of polystyrene–polydiene (isoprene or butadiene) diblock, triblock, and star-block copolymers. A representative phase diagram, summarizing the results of various studies based on polystyrene–polyisoprene (PS–PI) diblock copolymers is presented in Figure 1a; similar phase diagrams are found for the other molecular architectures. Four microstructures characterize ordered PS–PI melts: spherical microdomains arranged on a body-centered cubic lattice (bcc), hexagonally packed cylinders (H), an ordered bicontinuous double-diamond structure (OBDD), and lamellae (L). Varying the microstructure can be accomplished by changing f. To the best of our knowledge, there are no prior publications that report order–order transitions based on changing temperature alone.[2] This point is reflected in the vertical lines separating different ordered phases in Figure 1. At sufficiently small values of χN block copolymer melts disorder. The order–disorder transition (ODT) can be approached by varying either the temperature (in general, $\chi = AT^{-1} + B$ where A and B are system-specific constants) or the degree of polymerization.

Most of the features found in Figure 1a can be qualitatively, and in some cases quantitatively, accounted for theoretically. For $\chi N \gg 10$, the so-called strong segregation limit (SSL), predictions by Helfand[3] and others[4,5] accurately describe the microdomain period and size, with the exception of the OBDD phase, which has not been predicted to date.[6] Near the ODT, frequently

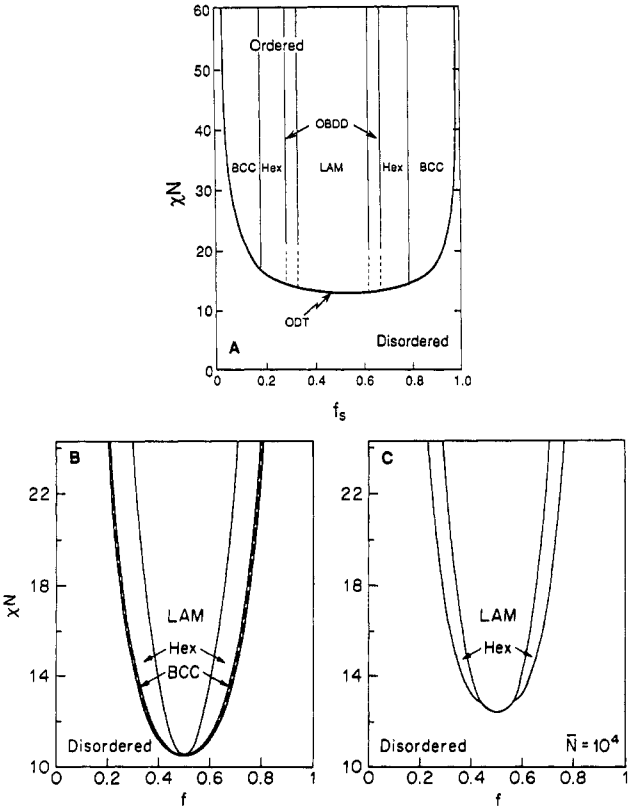

Figure 1. (a) Experimental phase diagram for polystyrene–polyisoprene (PS–PI) diblock copolymers.[29] (b) Theoretical mean-field phase diagram for diblock copolymers.[1,7] (c) Fluctuation-corrected mean-field phase diagram.[1,8]

† Current address: Risø National Laboratory, Roskilde, Denmark.

0024-9297/92/2225-1743$03.00/0

referred to as the weak segregation limit (WSL), the theories have been somewhat less successful. Mean-field theory, first developed by Leibler,[7] anticipates curved order–order transition boundaries that converge on a critical point at $f = {}^1/_2$ and $\chi N = 10.5$ as illustrated in Figure 1b. Fredrickson and Helfand[8] have corrected Leibler's result for fluctuation effects (Figure 1c), following a procedure developed by Brazovskii,[9] leading to the termination of the order–order transition lines at a fluctuation-induced first-order ODT. The fluctuation theory has been quantitatively verified in the disordered state for both symmetric[10,11] and asymmetric[12] diblock copolymers. However, only a limited number of experiments have been conducted on ordered block copolymers near the ODT, where the fluctuation theory is most applicable (for this reason the order–order transition lines near the ODT are indicated by dashed lines in Figure 1a).

Motivated by these observations and evidence of fluctuation effects in nearly symmetric lamellar specimens,[11] we have prepared a series of asymmetric poly(ethylene-propylene)–poly(ethylethylene) (PEP–PEE) diblock copolymers in order to investigate the effects of fluctuations in other parts of the block copolymer phase diagram. PEP–PEE polymers are attractive materials for this purpose because the χ parameter is relatively small, leading to an order–disorder transition at nearly ideal molecular weights[11] (too high a molecular weight makes small-angle scattering and rheological measurements difficult, while low molecular weight polymers are not suitable for comparison with the statistical theories). We will describe our results for $f = 0.75$ (here f refers to the volume fraction of PEP) in a separate publication.[12]

In this paper we present our initial findings based on small-angle neutron scattering (SANS) and rheological measurements for $f = 0.65$. Our choice of this composition was guided by the conflicting predictions of mean-field and fluctuation theory, both of which differ from the experimental (PS–PI) results (see Figure 1). On the basis of the latter, we anticipated a single ordered phase (OBDD or lamellar) that would disorder at an elevated temperature. Mean-field theory leads us to expect a L-to-H-to-bcc sequence of order–order transitions followed by an ODT, while fluctuation theory predicts a L-to-H transition and then a disordering transition. None of these expectations was realized for the $f = 0.65$ PEP–PEE sample. Although we do find that ordered lamellae pass through two intermediate ordered phases prior to disordering, these middle phases are not hexagonally packed cylinders or bcc spheres. This discovery leads us to question the concept of a universal block copolymer phase diagram based solely on χN and f.

Experimental Section

A *cis*-1,4-polyisoprene–1,2-polybutadiene (PI–PB) diblock copolymer was synthesized using anionic polymerization techniques described in a previous publication.[13] The product was subsequently saturated by separate reactions with hydrogen and deuterium gas (500 psi) over a palladium catalyst supported on calcium carbonate (Strem) in a dilute cyclohexane solution (2% w/v) maintained at 70 °C, yielding a poly(ethylenepropylene)–poly(ethylethylene) (PEP–PEE) diblock copolymer. A discussion of this reaction is presented elsewhere.[14] Deuteration of *cis*-1,4-polyisoprene and 1,2-polybutadiene under these conditions does not lead to the stoichiometric addition of two deuterons to each double bond. In separate reactions with comparable molecular weight homopolymers we find that on average four to five deuterons are associated with each isoprene repeat unit, while only two to three deuterons are found on a butadiene moiety; these values are obtained from density gradient column measurements. Such isotope exchange reactions are well-known in the field of heterogeneous catalysis. As a result of this asymmetric addition of deuterium to the individual blocks of the polydiene block copolymer, the deuterated PEP–PEE product contains an excess of deuterium on the PEP block that serves to introduce a modest level of neutron contrast (see below). Except where stated otherwise, the remainder of this paper deals with the deuterated material.

Based on nearly complete conversion (>99%) of the diene monomers and a highly efficient saturation (>99.5% by ^{1}H NMR), the composition of the PEP–PEE material was established to be 65% by weight PEP. The PI and PB microstructures were determined previously[13] by ^{13}C NMR to be 75% cis-1,4, 20% trans-1,4, and 5% 3,4 and >99% 1,2, respectively. Hence, the PEP block contains a random distribution of 95% ethylene-propylene and 5% isopropylethylene repeat units, while the PEE block contains essentially all atactic ethylethylene repeat units.

A weight-average molecular weight of 94 000 was obtained from light scattering measurements conducted with THF as the solvent. Size-exclusion chromatography (SEC) measurements, conducted with THF as the mobile phase, indicate a polydispersity of $M_W/M_N = 1.05$; the SEC instrument was calibrated with a set of $f = 0.55$ PEP–PEE diblock copolymers.[13] There was no homopolymer evident in the SEC traces, indicating that less than 2% of the living PI blocks were terminated during the block copolymer synthesis.

Rheological experiments were conducted using a Rheometrics RSA II dynamic mechanical spectrometer operated in the simple shear geometry. Specimens were prepared by heating in a vacuum oven (10^{-1} Torr) to 180 °C while compressing the material between Teflon-covered plates. Pieces 0.5 mm thick were then placed on either side of the shear-sandwich fixture and mounted on the mechanical spectrometer. Two separate sample preparation procedures were used. In both cases the specimens were heated above the order–disorder transition (ODT), $T_{ODT} = 175$ °C (see the following sections) and subsequently cooled to a lower temperature. Application of a 100% oscillatory strain at low frequencies ($0.06 \leq \omega \leq 1$ rad/s) while cooling at 0.5 °C/min to ca. 120 °C was found to produce macroscopically oriented microstructures as described in the following sections. Cooling from the disordered state without application of a shear field leads to a macroscopically isotropic ordered material. The dynamic elastic (G') and loss (G'') moduli were determined for the shear-oriented and isotropic materials as a function of frequency ($10^{-2} \leq \omega \leq 10^2$) and temperature ($20 \leq T \leq 180$ °C) while subjected to a 2% strain amplitude.

Small-angle neutron scattering (SANS) specimens were oriented in a shearing apparatus similar to that described by Hadzioannou et al.[15] Square sheets of block copolymer 1 mm thick by 5 × 5 cm^2 were subjected to an oscillatory strain (100% strain amplitude at 0.06 rad/s) while cooling at 1 °C/min from 175 to 75 °C. Strips 1 mm wide were cut from the oriented sheet and mounted between ${}^1/_{16}$-in. quartz disks and sealed with epoxy while under an argon atmosphere. Three sets of SANS specimens were prepared with orientations established by the shearing coordinate system as illustrated in Figure 2.

SANS experiments were performed at the Risø National Laboratory located in Roskilde, Denmark, using $\lambda = 6.0$-Å wavelength neutrons ($\Delta\lambda/\lambda = 0.17$) and pinhole collimation. The sample-to-detector distance was 6 m, and scattering events were recorded on a 60 × 60 cm^2 area detector that was corrected for variations in sensitivity and background scattering. SANS intensities are reported in arbitrary units.

Results

The viscoelastic properties of PEP–PEE block copolymers have been shown to be strongly correlated with phase behavior.[10-12,16] This has facilitated the accurate determination of the order–disorder transition which is characterized by significant discontinuties in G' and G'' at low frequencies (i.e., $\omega \lesssim \omega_c$ where ω_c^{-1} is roughly 10 times the single-chain terminal relaxation time).[16] We have exploited this technique in the present study in order to identify order–order transitions in the $f = 0.65$ PEP–PEE diblock copolymer. Figure 3 illustrates the temperature

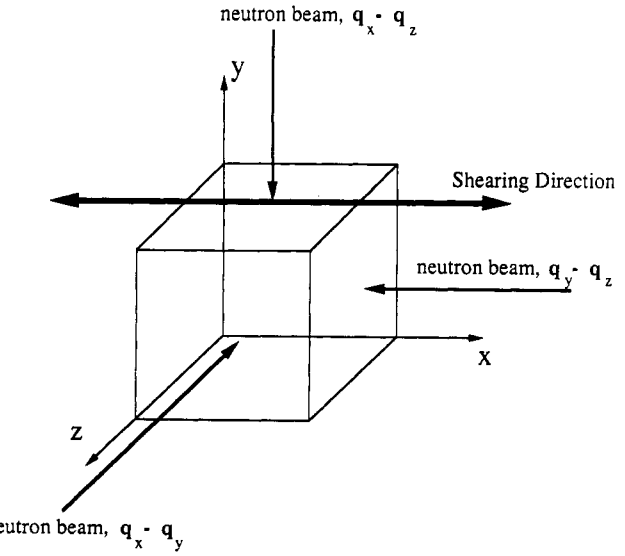

Figure 2. Experimental geometry for sample shear orientation and dynamic mechanical measurements and small-angle neutron scattering (SANS) experiments.

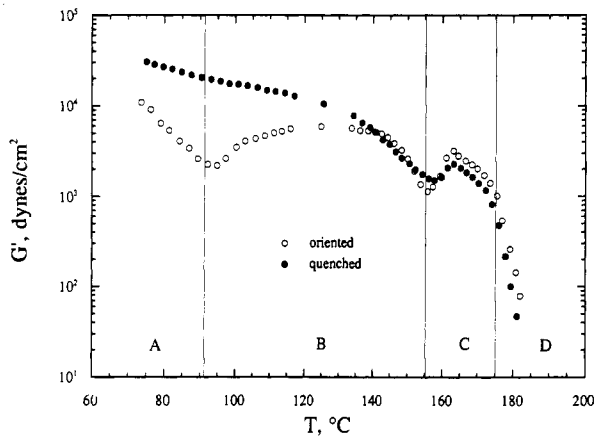

Figure 3. Dynamic elastic shear modulus obtained at a constant frequency (ω = 0.1 rad/s) while heating. The oriented specimen was obtained by shearing the material while cooling from 180 °C. Four regions (A–D) corresponding to four distinct phases can be identified in the oriented spectra.

dependence of G' obtained under isochronal conditions (ω = 0.1 rad/s). At the lowest measurement temperatures, the shear-oriented specimen displays a characteristic decrease in elasticity with increasing temperature, which is typical of an ordered block copolymer.[16] At 91 °C this trend is abruptly reversed and the modulus increases. As the temperature continues to increase, G' reaches a maximum value and again decreases. A second abrupt reversal of this behavior occurs at 155 °C, leading to a second peak in G'. At about 175 °C, the opposite effect is observed, with the dynamic elastic modulus dropping abruptly. This final effect can be associated with the ODT as shown in several prior publications.[10-12,16] As detailed below, this complex rheological behavior derives from the existence of four equilibrium phases in sample PEP–PEE-9, denoted A–D, as delineated by the vertical lines in Figure 3.

The changes in the isochronal $G'(T)$ data evident in Figure 3 are also manifested in $G'(\omega)$ as illustrated in Figure 4. Representative isothermal frequency scans taken from each of the four temperature regimes indicated in Figure 3 show qualitatively different low-frequency responses. (Note, these results have been time–temperature superposed using the $\omega > \omega_c$ data.) At 63 °C $G'(\omega)$ is nearly terminal despite the fact that this is an ordered material.

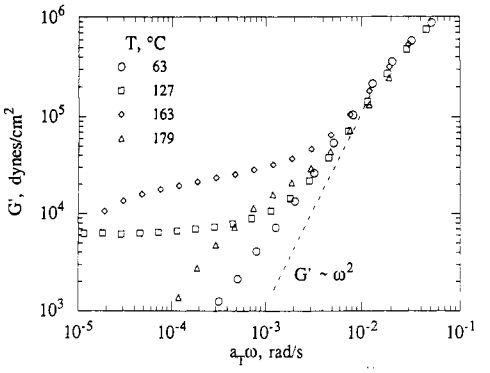

Figure 4. Representative dynamic elastic shear modulus obtained while heating a shear-oriented specimen. The dashed line represents the anticipated high-temperature terminal response. These data have been time-temperature superimposed based on the high frequency response. Variations in $G'(\omega)$ with temperature reflect changes in microstructure.

This result can be attributed to the long-range order induced by shearing (see below). Increasing the temperature to 127 °C leads to a dramatic increase in G' and a qualitatively different frequency dependence below ω_c. Raising the temperature to 163 °C further increases G' although the frequency dependence is not significantly altered. Finally, at 179 °C $G'(\omega)$ becomes nearly terminal ($G' \sim \omega^2$) although a sizeable deviation from the high-temperature behavior (dashed line), attributable to composition fluctuations,[11,16] is clearly evident. These trends are also reflected in G'' although the low-frequency limit is more difficult to access since $\omega_c'' < \omega_c'$.[16]

Specimens cooled below T_{ODT} in the absence of a shear field behave differently. Figure 3 contrasts the isochronal $G'(T)$ response of such a specimen (open symbols) with the previously described shear-oriented results (filled symbols). Without the benefit of the later it would be difficult to distinguish between the A and B regimes in the isotropic material. Above approximately 125 °C the specimens respond similarly and the transitions at 155 and 175 °C are plainly evident in both cases. These trends are also reflected in the isothermal frequency scans (not shown).

SANS measurements provide direct evidence of the changes in microstructure that accompany the rheological transitions described above. Scattering data, obtained at four temperatures, representative of each of the four rheologically distinct regions indicated in Figure 3, are presented in Figures 5–8. Each of these illustrations (except Figure 8) contain three 3-dimensional scattering plots along with the associated 2-dimensional contour plots. The orientation of the sheared specimens with respect to the incident neutron beam is depicted in Figure 2. For example, with the beam directed along the x (i.e., shearing) direction, the $\mathbf{q}_z$–$\mathbf{q}_y$ scattering plane is accessed where $|\mathbf{q}| = q = 4\pi\lambda^{-1}(\sin\Theta/2)$ is the magnitude of the scattering wavevector (λ and Θ are the neutron wavelength and scattering angle, respectively).

Within each of these figures the 3-dimensional plots are drawn to (relative) scale. In order to facilitate comparison of SANS results obtained at different temperatures, we have normalized these results to produce a common maximum intensity at each temperature; the relative scale factors are 1× at 50 °C, 11.9× at 124 °C, and 18.3× at 164 °C (note the data at 179 °C was obtained on separate specimens and could not be quantitatively scaled to the other results). All the contour plots have been normalized so as to exhibit the same number of level lines in order to emphasize variations in scattering symmetry.

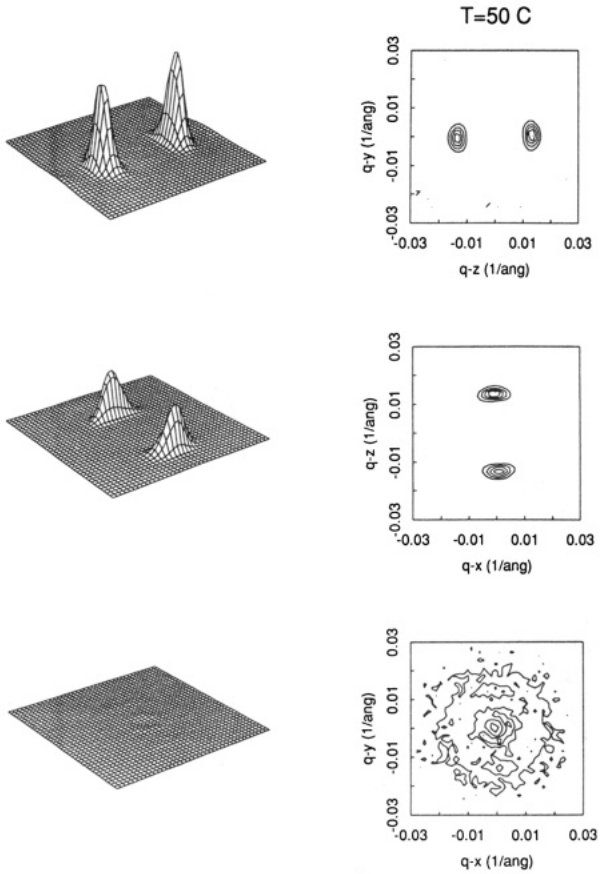

Figure 5. Representative SANS patterns obtained with three neutron bean orientations (see Figure 2) for phase state A. 3D plots are drawn to relative scale. 2D contour plots are each normalized to obtain a constant number of level lines. Careful inspection of the $\mathbf{q}_x$–$\mathbf{q}_y$ contour plot reveals a weak pair of reflections.

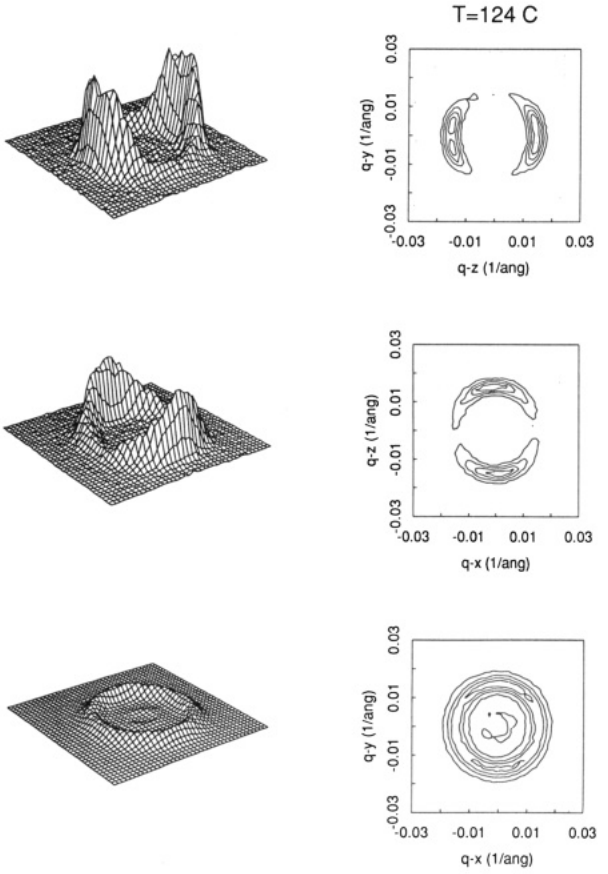

Figure 6. Representative SANS patterns obtained with the same neutron beam orientations used in Figure 5 for phase state B. 3D plots are drawn to relative scale and multiplied by a factor of 11.9× with respect to Figure 5. 2D contour plots have been normalized as in Figure 5.

An alternative method of evaluating the SANS results is to azimuthally average, thereby reducing the 3-dimensional data to the 2-dimensional form of intensity I versus q. $I(q)$ is plotted in Figure 9 for the SANS data shown in Figures 5–7. Although this procedure ignores the inherent anisotropy in these scattering patterns, it does provide an efficient means of comparing the overall scattering intensity from a sizeable number of data sets.

The azimuthally averaged data are particularly useful for locating the temperature where the transition between scattering patterns occurs. For this purpose we focus on the average peak intensity, $I(q^*)$.[17] This parameter was obtained by best-fitting modified Lorentzian or Gaussian functions to the azimuthally averaged data. The results for two specimen orientations, $I(q^*_{zy})$ and $I(q^*_{yx})$, are presented as a function of temperature in Figure 10. Upon heating from room temperature, there is an abrupt increase and decrease in $I(q^*_{zy})$ and $I(q^*_{yx})$, respectively, at 91 °C. This corresponds to the A ↔ B transition temperature observed rheologically. Significantly, this transition is completely reversible as illustrated in Figure 11 (here we note that the G' data shown in Figure 11 were obtained from the fully protonated specimen[18]). $G'(\omega \ll \omega_c')$ displays a hysteresis loop, centered around 96 °C, consistent with a first-order transition that is traversed at finite heating and cooling rates (≈0.2 °C/min). A similar trend is found in the SANS measurements as illustrated by $I(q^*_{yx})$ measured during a heating and cooling cycle (≈0.05 °C/min). Because the SANS measurements were conducted over a considerably longer period of time (completion of a hysteresis loop required several hours by SANS versus less than 1 h rheologically), the corresponding hysteresis loop is predictably narrower. Furthermore, the anisotropic 3-dimensional scattering patterns depicted in Figures 5 and 6 can be cycled repeatedly. In fact, Figure 5 represents scattering results obtained after cooling specimens from state B. Because this transition is completely reversible (with respect to long-range orientation), we refer to it using a double-directed arrow, i.e., A ↔ B.

At approximately 155 °C, a second first-order transition occurs as evidenced by a discontinuous variation in $I(q^*_{zy})$ and $I(q^*_{yx})$ (Figure 10) and a clear change in the scattering symmetry (see Figures 6 and 7). These effects coincide with a transition in G' as seen in Figure 3. However, unlike the A ↔ B transition, once the specimens have been heated above 155 °C, the original long-range order characterizing state B cannot be fully recovered by cooling, leading us to refer to this transition with a single-directed arrow, i.e., B → C. This irreversibility is clearly reflected in $I(q^*_{zy})$, which fails to return to its original lower temperature value upon cooling as shown in Figure 10.

At 175 °C, a third first-order transition occurs, leading to three equivalent azimuthally symmetric scattering patterns. This transition coincides with the order–disorder transition (ODT) identified rheologically (Figure 3). The SANS results above 175 °C are consistent with a disordered, isotropic fluid state. Long-range order cannot be obtained by cooling the disordered melt in the absence of a shear field,[1] and accordingly we refer to the highest temperature transition as C → D.

Increasing temperature also leads to a decrease in q^*. This is primarily due to the negative thermal expansivity of PEP and PEE; $d \ln R_g^2/dT = -2.3 \times 10^{-4}$ and $-1.3 \times$

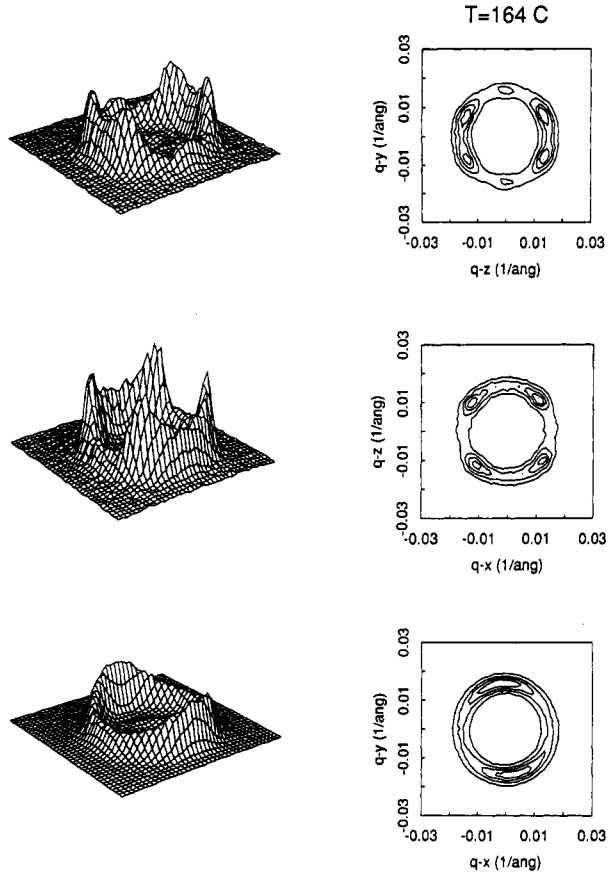

Figure 7. Representative SANS patterns obtained with the same neutron beam orientation used in Figures 5 and 6 for phase state C. These results were obtained by heating the specimens used to obtain Figure 6. 3D plots are drawn to relative scale and multiplied by a factor 18.3× with respect to Figure 5. 2D contour plots have been normalized as in Figure 5.

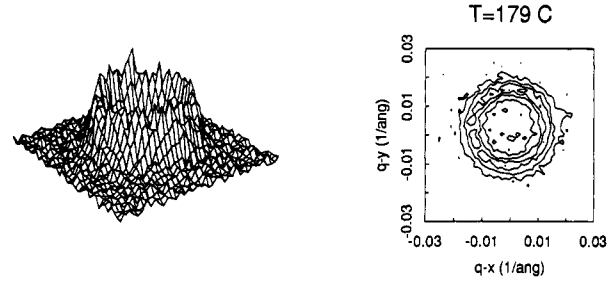

Figure 8. Disordered (phase state D) SANS pattern obtained by heating a shear-oriented material through the order–disorder transition. The results obtained with $\mathbf{q}_x$–$\mathbf{q}_z$ and $\mathbf{q}_y$–$\mathbf{q}_z$ beam orientations are indistinguishable from those shown. These data are not calibrated in intensity relative to the results shown in Figures 5–7.

10^{-4} K^{-1}, respectively.[11] Similar behavior is found with lamellar ($f = 0.55$)[11] and cylindrical ($f = 0.77$)[12] PEP–PEE diblock copolymer microstructures. Furthermore, there is no variation in dq^*/dT or discontinuity in q^* at the order–disorder transition in these materials.

The results presented in this section have been selected from extensive sets of rheological and SANS measurements in order to establish the existence of four equilibrium phases in $f_{PEP} = 0.65$, $M_w = 94\,000$ PEP–PEE diblock copolymer. To the best of our knowledge such phase complexity is unprecedented in block copolymer melts. In the following sections we examine these findings in an effort to identify the associated microstructures.

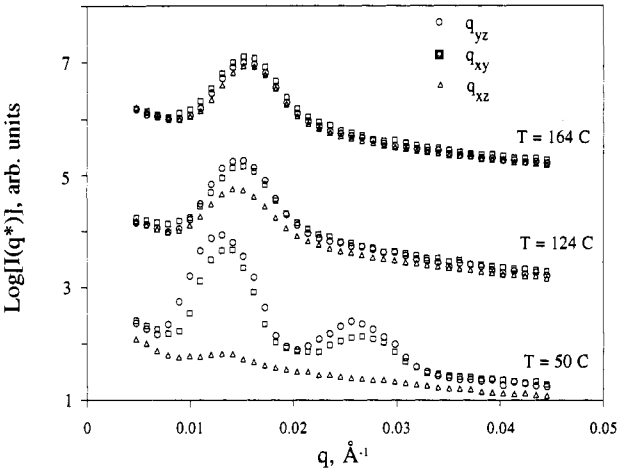

Figure 9. Azimuthal averages of data shown in Figure 5 (T = 50 °C), Figure 6 (T = 124 °C), and Figure 7 (T = 164 °C).

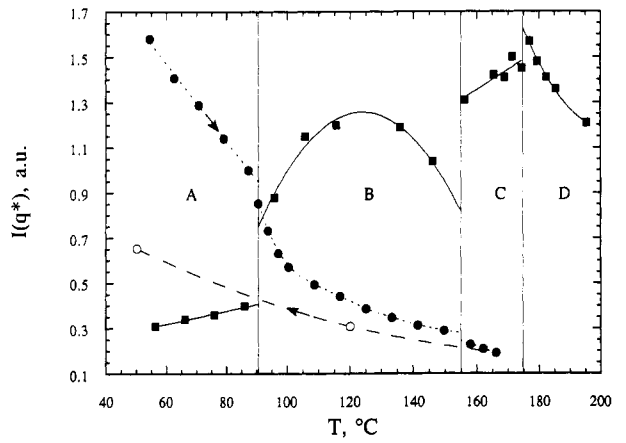

Figure 10. Azimuthally averaged peak scattering intensities $I(q^*_{yz})$ (●,○) and $I(q^*_{xy})$ (■). Filled symbols correspond to data obtained while heating shear-oriented specimens. The open symbols refer to data obtained while cooling and illustrate the reversible nature (with respect to microstructural orientation) of the B → C phase transition.

Analysis

The results presented in the previous section clearly demonstrate that $f = 0.65$ (volume % PEP) PEP–PEE diblock copolymers are characterized by a complex phase behavior near the order–disorder transition. Three phase transitions are evident in the rheology and SANS data: order–order transitions at approximately 91 °C (A ↔ B) and 155 °C (B → C) and an ODT (C → D) at 175 °C where the arrows signify the directions that preserve long-range order (see the previous section). As described below, we can assign microstructures to the lowest and highest temperature phases, A and D, respectively, as illustrated in Figure 12. Despite having essentially single-crystalline SANS data we cannot unambiguously establish the microstructures of phases B and C. Nevertheless, on the basis of the analysis that follows, we associate phase B with a perforated-lamellar microstructure and speculate that phase C constitutes an ordered bicontinuous phase, as indicated in Figure 12. Before examining the rationale behind these assignments we must emphasize the tentative nature of our conclusions regarding phases B and C. While the evidence supporting the existence of four distinct equilibrium phases is decisive, there is inadequate information at present to establish the exact microstructure of the two middle phases. The remainder of this section is divided into four parts that deal with phases A–D individually.

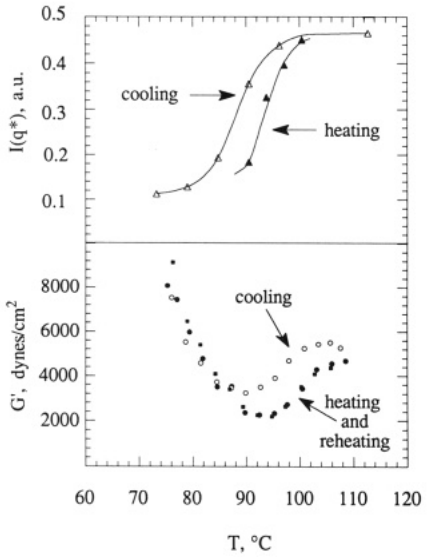

Figure 11. (a) Azimuthally averaged peak scattering intensities $I(q^*_{yz})$ obtained upon heating and cooling a shear-oriented specimen through the A ↔ B phase transition. (b) Isochronal dynamic elastic moduli associated with the A ↔ B transition. These results demonstrate the reversibility of this order–order transition.

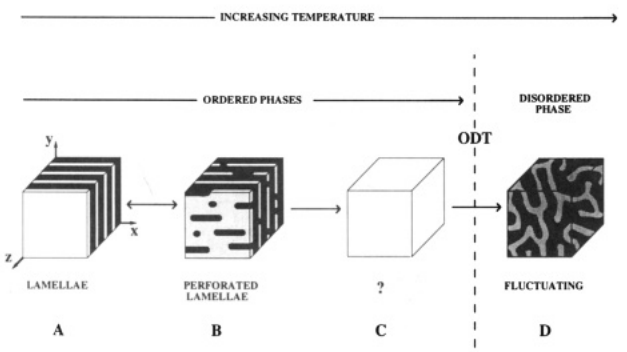

Figure 12. Four phases identified for the $f = 0.65$ PEP–PEE diblock copolymer. The (rippled) lamellae (A) and disordered state (D) microstructures are firm assignments based on the SANS data presented in Figures 5 and 9 and in ref 11, respectively. SANS and rheological measurements support a tentative perforated-lamellar microstructure for phase B. A specific microstructure cannot be assigned to ordered phase C. However, the rheological data suggest a bicontinuous morphology. The decrease in contrast with increasing temperature signifies a reduction in the compositional variation between microdomains. Above the ODT (phase D) the morphology fluctuates both spatially and temporally.

Phase A. The lowest temperature phase can be definitively associated with a lamellar microstructure. Scattering in the $\mathbf{q}_z$–$\mathbf{q}_y$ and $\mathbf{q}_x$–$\mathbf{q}_z$ planes (Figure 5) is dominated by a pair of reflections indicative of lamellae oriented parallel to the x–y plane (see Figure 2) as shown in Figure 12. This is reinforced by the near complete absence of scattering in the $\mathbf{q}_y$–$\mathbf{q}_x$ plane. Final confirmation of this assignment can be found in the $I(q)$ data presented in Figure 9. Second-order reflections are evident at $2q^*$ with the neutron beam directed along the x and y directions; absence of third-order reflections at $3q^*$ can be attributed to an extinction condition at $f = {}^2/_3$.[19] Unexpectedly, the lamellae are oriented perpendicular to the plane of shear (Figures 2 and 12) contrary to what is found with nearly symmetric PS–PI[20] and PEP–PEE[11] block copolymers. We well return to this point in the following section.

While the assignment of a lamellar microstructure to phase A is rather unambiguous, there are several peculiar features in the SANS data that should be noted. The strong reflections found in Figures 5 and 9 are unequal in peak width and integrated intensity (also reflected in Figure 9) and are azimuthally broadened (particularly in the $\mathbf{q}_z$–$\mathbf{q}_x$ plane). Inhomogeneities in the shearing field, and sample deformation during cutting and mounting in the SANS cells, along with the slight misalignment in the neutron scattering instrument could contribute to these differences. An alternative cause may be small-amplitude undulations (ripples) in the lamellae. Ripple phases are known to occur in certain lyotropic liquid-crystalline materials.[21] A possible ripple geometry, similar to that proposed by Goldstein and Leibler[21] for lipophilic bilayers, would involve undulating sheets of PEP separated by wavy sheets of PEE. In the absence of shearing patches of ripples would form with random orientation in the x–y plane. Careful inspection of the $\mathbf{q}_y$–$\mathbf{q}_x$ plot in Figure 5 reveals a very weak pair of reflections located at $|\mathbf{q}_y^*|$, that produce the small peak in $I(q_{xy})$ seen in Figure 9. This suggests that the ripples have been preferentially oriented coincident with the shear (x) axis; the significance of this point will become obvious in the following analysis of the B and C phases.

The rheological properties of the oriented lamellar phase (same orientation as indicated in Figures 2 and 12) are similar to that of a homopolymer melt. G'' is proportional to ω (not shown), and G' is nearly terminal (Figure 4), deviating only slightly from a liquidlike response ($G \sim \omega^2$) at the lowest measurement frequencies. This behavior is in marked contrast with the low-frequency response obtained previously from unoriented lamellar samples, $G' \sim G'' \sim \omega^{1/2}$.[16,22] The steep frequency dependence of G' (Figure 4) accounts for the steep temperature dependence of G' measured at constant frequency (see Figure 2). Apparently, with the lamellae oriented perpendicular to the shear plane, the mobility of the block copolymers is almost unaffected by the ordered structure. This surprising result may be a consequence of the proximity to the ODT which leads to a diffuse interfacial region and weakly localized block joints.

Phase B. At approximately 91 °C the PEP–PEE specimen undergoes a first-order phase transition. The intensities of the reflections in the $\mathbf{q}_z$–$\mathbf{q}_y$ and $\mathbf{q}_x$–$\mathbf{q}_z$ planes decrease dramatically and broaden around $\mathbf{q}^*$, and an anisotropic ring of scattering appears at q^* in the $\mathbf{q}_y$–$\mathbf{q}_x$ plane (Figure 6). A qualitative change in the rheological properties accompanies these structural rearrangements. What was nearly liquidlike behavior transforms into a solidlike response, $G' \sim \omega^0$ (Figure 4). These changes are discontinuous (Figures 3 and 10) and completely reversible (Figure 11).

We cannot unambiguously assign a microstructure to this lower temperature middle phase with the data presently available. However, these results strongly suggest two related possibilities. The first is a more pronounced ripple phase, similar to that described for phase A but with a greater amplitude. Such a buckling transition would qualitatively account for the SANS results. The curvature introduced to the lamellae would be expected to broaden the $\mathbf{q}_z$–$\mathbf{q}_y$ and $\mathbf{q}_x$–$\mathbf{q}_z$ reflections and introduce anisotropic scattering in the $\mathbf{q}_y$–$\mathbf{q}_x$ plane. It could also lead to the elimination of the $2q^*$ reflections as found in Figure 10. However, it seems unlikely that a ripple phase would exhibit grossly different rheological properties from the lamellar state as is seen in Figure 4. The solidlike G' suggests a more drastic structural rearrangement.

An alternative model that retains all the attributes of the ripple phase, with respect to the SANS results, is a perforated-lamellar structure. This can be created by simply increasing the magnitude of the ripple phase undulations until a set of passages perforate the minority component (i.e., PEE). This leaves the majority component (i.e., PEP) with its original 2-fold symmetry axis intact so that with cooling macroscopically oriented lamellae can be recovered. On the basis of the SANS data alone, we cannot discriminate between these two models. However, the rheological results favor the perforated-lamellar microstructure, which is characterized by a 3-dimentional interface network that could account for the observed increase and frequency dependence of G'. Accordingly, this microstructure is depicted in Figure 12B. A catenoid-lamellar microstructure[23] would result in the limit of a dense array of cylindrically symmetric perforations. Cubic or hexagonal packing of catenoids would be manifested in the $\mathbf{q}_x$–$\mathbf{q}_y$ scattering plane as 4- or 6-fold reflections. Because these are not observed (Figure 6), we have depicted the perforations with variable aspect ratios.

At this point it is useful to return to the issue of shear orientation. The specimens studied in this work were aligned by large-amplitude shearing at 100 °C, i.e., in phase B. If the equilibrium structure at this temperature is in fact perforated-lamellae, it seems unlikely that this morphology, with its solidlike elasticity, would survive the shearing process. Instead, something more fluidlike would be generated under the large deformation conditions. One possibility is the ripple phase. Ripples would preferentially orient parallel to the shearing direction (analogous to rods) and could be responsible for the ultimate vertical lamellae orientation and weak oriented ripples observed at lower temperatures. With the cessation of shearing, the perforations would be expected to grow back from the existing undulations. Another attractive feature of this hypothesis is that it naturally introduces a broken symmetry in the y–x plane which is necessary to explain the anisotropy in the $\mathbf{q}_y$–$\mathbf{q}_x$ scattering at 124 °C (see the contour plot in Figure 6) and the evolution of broken symmetries at 164 °C (see below). The growth of perforations from oriented ripples in the lamellar phase naturally leads to preferred correlations between such perforations along the original shearing direction.

Phase C. Heating the block copolymer specimen above 155 °C produces a second first-order phase transition that is reflected in all the SANS and rheological measurements. G' increases by 2–3 times over a wide range of reduced frequencies (Figures 3 and 4). $I(q^*)$ decreases and increases in the z–y and y–x planes, respectively, leading to a nearly orientation-independent average peak intensity as shown in Figure 9c. But the most striking changes are found in the 3-dimensional SANS plots shown in Figure 7.

In the z–y scattering plane six distinct reflections are associated with phase C, arranged with hexagonal symmetry at q^*. Four of these, which evolve from the two crescent-shaped reflections associated with the lower temperature B phase (Figure 6), are more intense than the other two, leading to an overall 2-fold symmetry axis. The two reflections characterizing the x–z scattering plane at 124 °C (Figure 6) each spawn two new SANS peaks in the C phase that are arranged with square symmetry at q^*. However, these peaks are asymmetric and the overall scattering pattern also exhibits a 2-fold symmetry axis. In the y–x scattering plane, the subtle anisotropy in $I(q_{yx})$ at 124 °C increases markedly with heating through the B → C transition, leading to a well-defined 2-fold symmetry.

At present we cannot assign a unique microstructure to phase C. Although the specimen obviously retains a "single-crystalline" form, scattering reflections are observed only at q^* (see Figure 9). We attribute the lack of higher order reflections to a nearly sinusoidal composition profile which would produce such a result. Without the benefit of higher order reflections, indexing the lattice based on the SANS data available is not possible. What can be concluded is that the microstructure is neither lamellae nor hexagonally packed cylinders, since neither of these structures would produce the complement of scattering patterns found in Figure 7.

Although we are not able to conclusively identify phase C, we suspect it is an ordered bicontinuous microstructure.[30] Particularly noteworthy is the increase in G' relative to phase B. If our speculation regarding phase B is correct, then this 2–3-fold jump in elasticity can be associated with the creation of an additional interfacial structure. One means of doing so would be to create additional passages in the PEP domains of the monocontinuous perforated-lamellar structure, thereby producing a bicontinuous ordered structure. Such a structural rearrangement would also disrupt the 2-dimensional plane characterizing the perforated-lamellar microstructure (black microphase in Figure 12B), which would explain why the B → C phase transition is irreversible with respect to long-range order. Once the lower symmetry phases (A and B) have transformed to a higher symmetry state (phase C) recovery of long-range order requires the application of a symmetry breaking field, such as shearing. For the same reasons, shearing is required when a disordered melt (the highest symmetry phase) is cooled into any of the ordered states if long-range order is desired.

Although we cannot recover a fully oriented material by cooling a single-crystalline specimen through the B → C transition, the actual phase behavior does not require long-range order. This is best seen in the isochronal measurements of G' (Figure 3) for shear-oriented and isotropic specimens. Thermodynamically the B → C order–order transition is fully reversible. That the isotropic and single-crystalline forms of phase C are rheologically similar is also consistent with a bicontinuous microstructure, which would display solidlike properties regardless of microstructure orientation or processing history. In contrast, the rheological properties of the lamellar microstructure of phase A are highly dependent on long-range order and specimen orientation. Whereas the vertically oriented lamellar (see Figure 12) are nearly liquidlike (Figure 4), the polycrystalline morphology, produced by cooling a disordered melt in the absence of shearing, exhibits a dramatically higher, nonterminal elastic behavior as described in earlier studies.[16,22] This obscures the rheological manifestation of the A ↔ B transition in isotropic specimens.

Phase D. At 175 °C the PEP–PEE block copolymer disorders. The dynamic elastic modulus drops (Figure 3), becoming nearly terminal at the lowest measurement frequencies, $G' \sim \omega^{1.7}$ (Figure 4). Fluctuation effects are clearly manifested in the low-frequency rheological response at 179 °C, evidenced by a displacement of the terminal regime to significantly lower frequencies than would characterize a spatially homogeneous melt, i.e., for $T \gg T_{ODT}$ as indicated by the dashed curve. The SANS patterns at 179 °C are azimuthally symmetric and equivalent for all three scattering orientations, further confirming that this polymer is a disordered, isotropic fluid. These characteristics closely resemble those previously

associated with a bicontinuous fluctuating disordered state in a $f = 0.55$ PEP–PEE diblock copolymer.[11] By analogy, we can assign a similar morphology to the $f = 0.65$ material just above the ODT as illustrated in Figure 12D.

Discussion

The primary purpose of this publication is to report our discovery of four equilibrium phases in a single block copolymer melt. This represents a departure from current theory and experiment as summarized in Figure 1. Superficially these results might appear to be consistent with the mean-field theory of Leibler,[7] where multiple ordered phases are predicted. However, the two middle phases, between the lamellar and disordered states, are definitely not hexagonally packed cylinders, or bcc spheres, obviating such a comparison. (Recent modifications of Leibler's theory have led to the prediction of more complex microstructures. Olvera de la Cruz et al.[24] report a narrow range of compositions ($0.47 < f < 0.52$) where the catenoid-lamellar microstructure is stable below the ODT). Furthermore, as shown in a separate publication,[12] $f = 0.75$ PEP–PEE specimens exhibit a hexagonal-to-disorder transition, ruling out the existence of a bcc phase near the ODT, even at this more asymmetric composition. While the fluctuation theory does not account for our results in its current form, a free-energy competition based on the new (and as yet ill-defined) ordered state symmetries could in principle lead to a viable prediction.

More significance can be placed on a comparison of the PEP–PEE phase diagram with that characterizing PS–PI diblock copolymers (Figure 1a). Here the concept of a universal block copolymer phase diagram is directly tested. We are not aware of any published reports of order–order transitions in the polystyrene–polydiene system[2] although relatively few studies have been conducted near the ODT for $f = 0.65$ or $f = 0.35$. This leads us to tentatively conclude that all block copolymer phase behavior cannot be reduced onto a single universal phase diagram based solely on the parameters f, χ, and N.

While it is premature to examine the molecular origins of the multiple ordered phase behavior exhibited by the PEP–PEE polymer in any detail, several observations can be made. Our choice of composition in this study was influenced in part by the recognition that various cubic phases have been documented to occur between the hexagonal and lamellar phases of certain lyotropic liquid-crystalline materials.[25-28] The OBDD phase conforms to this pattern, which is unlikely to be merely a coincidence. Despite the obvious similarities between block copolymers, lyotropic liquid crystals, microemulsions, and other such systems, there have been relatively few attempts to rationalize the similarities and differences exhibited by these closely related mesomorphic materials. The polystyrene–polydiene phase diagrams are actually one of the least complex amongst the systems cited. Our observation of multiple ordered phases in an $f = 0.65$ PEP–PEE diblock copolymer represents a departure from the generally accepted universal behavior. This suggests that our understanding of block copolymers near the ODT is incomplete and that additional factors such as those encountered in other mesomorphic systems must be considered in developing a comprehensive theory for block copolymer phase behavior.

Obviously, interfacial curvature plays a crucial role in determining the microstructure of block copolymer melts as discussed by Thomas et al.[23] Until now, weak segregation limit theories have produced curvature through variations in f or χN leading to the familiar spherical, hexagonal, and lamellar phases. The effects of asymmetric block coil statistics (i.e., differences in the statistical segment length between blocks) have not been considered. Polymer coil dimensions are determined by the number and structure of the repeat units; for unperturbed (Gaussian) chains $R_g = \mathbf{a}(N/6)^{1/2}$ where R_g is the radius of gyration and the repeat unit structure is reflected in the statistical segment length $\mathbf{a}$. The ratio of statistical segment lengths for the two blocks $\mathbf{a}_A/\mathbf{a}_B$ of a diblock copolymer reflects the degree of configurational asymmetry that must be accommodated by a particular microstructure. Since $\mathbf{a}_A/\mathbf{a}_B$ is not directly related to the composition, $f = N_A/(N_A + N_B)$, such a configurational asymmetry may lead to a state of frustration[26] for certain values of f. For example, a compositionally symmetric ($f = 1/2$) lamellar morphology may not easily accommodate a highly asymmetric ($\mathbf{a}_A/\mathbf{a}_B > 1$) molecule, leading to the development of alternative structures such as ripple or perforated-lamellar phases as depicted in Figure 12. Clearly the tendency to form complex, interconnected microstructures will be enhanced by selecting a composition that readily supports a bicontinuous area minimizing surface such as that characterizing the OBDD phase. We suspect that the combination of a large configurational asymmetry, $\mathbf{a}_{PEP}/\mathbf{a}_{PEE} \cong 1.44$ ($\mathbf{a}_{PI}/\mathbf{a}_{PS} \cong 1.17$ where both values are calculated based on normalized, equal-volume repeat units), and our choice of composition, $f = 0.65$, produced the multiple ordered phases reported here. We will explore these issues in more detail in future publications.

Acknowledgment. Support for this research was provided by the Air Force Office of Scientific Research (AFOSR-90-0207) and the Center for Interfacial Engineering (CIE), a National Science Foundation Engineering Research Center at the University of Minnesota. Additional assistance has been provided to K.A. by the NATO Science Fellowship Programme, the Danish Natural and Technical Science Councils, and Knud Højgaards Foundation.

References and Notes

(1) Bates, F. S.; Fredrickson, G. H. *Annu. Rev. Phys. Chem.* **1990**, *41*, 525.
(2) A possible order–order transition in a polystyrene–polyisoprene diblock copolymer melt was reported by: Golbran, D. Ph.D. Thesis, University of Massachusetts, 1988.
(3) Helfand, E.; Wasserman, Z. R. In *Developments in Block Copolymers—1*; Goodman, I., Ed.; Applied Science: New York, 1982.
(4) Semenov, A. N. *Sov. Phys. JETP* **1985**, *61*, 733.
(5) Kawasaki, K.; Ohta, T.; Kohrogui, M. *Macromolecules* **1988**, *21*, 2972.
(6) Anderson, D. M.; Thomas, E. L. *Macromolecules* **1988**, *21*, 3221.
(7) Leibler, L. *Macromolecules* **1980**, *13*, 1602.
(8) Fredrickson, G. H.; Helfand, E. *J. Chem. Phys.* **1987**, *87*, 697.
(9) Brazovskii, S. A. *Sov. Phys. JETP* **1975**, *41*, 85.
(10) Bates, F. S.; Rosedale, J. H.; Fredrickson, G. H.; Glinka, C. J. *Phys. Rev. Lett.* **1988**, *61*, 2229.
(11) Bates, F. S.; Rosedale, J. H.; Fredrickson, G. H. *J. Chem. Phys.* **1990**, *92*, 6255.
(12) Almdal, K.; Bates, F. S.; Mortensen, K. *J. Chem. Phys.*, in press.
(13) Bates, F. S.; Rosedale, J. H.; Bair, H. E.; Russell, T. P. *Macromolecules* **1989**, *22*, 2557.
(14) Rosedale, J. H.; Bates, F. S. *J. Am. Chem. Soc.* **1988**, *110*, 3542.
(15) Hadziioannou, G.; Mathis, A.; Skoulios, A. *Colloid Polym. Sci.* **1979**, *257*, 136.
(16) Rosedale, J. H.; Bates, F. S. *Macromolecules* **1990**, *23*, 2329.
(17) This does not constitute a rigorous treatment since a phase transition could occur without a change in $I(q^*)$. A more quantitative evaluation of $I(q^*,\phi)$, where ϕ corresponds to the azimuthal angle, excludes the possibility of additional phase transitions. The use of $I(q^*)$ is simply the most efficient method of illustrating all three phase transition temperatures.

(18) The A ↔ B transition temperature is not strongly influenced by isotope labeling. The phase behavior near the ODT is more significantly affected by deuterium labeling.
(19) Shibayama, M.; Hashimoto, T. *Macromolecules* **1986**, *19*, 740.
(20) Hadziioannou, G.; Picot, C.; Skoulios, A.; Ionescu, M.-L.; Mathis, A.; Duplessix, R.; Gallot, Y.; Lingelser, J.-P. *Macromolecules* **1982**, *15*, 263.
(21) Goldstein, R. E.; Leibler, S. *Phys. Rev. Lett.* **1988**, *61*, 2213; *Phys. Rev. A* **1989**, *40*, 1025.
(22) Bates, F. S. *Macromolecules* **1984**, *17*, 2607.
(23) Thomas, E. L.; Anderson, D. M.; Henkee, C. S.; Hoffman, D. *Nature* **1988**, *334*, 598.
(24) Olvera de la Cruz, M.; Mayes, A. M.; Swift, B. W. *Macromolecules*, in press.
(25) Mariani, P.; Luzzati, V.; Delauoix, H. *J. Mol. Biol.* **1988**, *204*, 165.
(26) Anderson, D. M.; Gruner, S. M.; Leibler, S. *Proc. Natl. Acad. Sci. U.S.A* **1988**, *85*, 5364.
(27) Gruner, S. M. *J. Phys. Chem.* **1989**, *93*, 7562.
(28) Larsson, K. *J. Phys. Chem.* **1989**, *93*, 7304.
(29) Bates, F. S. *Science* **1991**, *251*, 898.
(30) **Note Added in Proof.** The SANS results obtained for phase C (Figure 7) are qualitatively consistent with an OBDD phase provided four equally probable microstructure orientations are present: the x, y, and z axes in Figure 1 corresponding to the [111], [1$\bar{1}$0], [11$\bar{1}$], the [111], [$\bar{1}$10], [$\bar{1}\bar{1}$1], the [$\bar{1}$11], [1$\bar{1}$0], [11$\bar{1}$], and the [$\bar{1}$11], [$\bar{1}$10], [$\bar{1}\bar{1}$1] directions, respectively, based on the coordinate system defined by Thomas et al. *Macromolecules*, **1986**, *19*, 2197. All the SANS peaks then represent {110} reflections. Growth of these microstructure orientations (which can be superimposed by 180° rotations around the [111] and [1$\bar{1}$0] directions) is consistent with the transformation of the oriented lower symmetry phase B to the higher symmetry OBDD state.